Ventilated partial cavitating flow around a blunt body near the free surface

Yiwei Wang, Xiaocui Wu, Chenguang Huang

Ventilated partial cavitating flow around a blunt body near the free surface

Yiwei Wang[1], Xiaocui Wu[1], Chenguang Huang[1]*

ISROMAC 2016

International Symposium on Transport Phenomena and Dynamics of Rotating Machinery

Hawaii, Honolulu

April 10-15, 2016

Abstract

Ventilated cavitation occurs as an extremely complicated problem if the free surface is close to the cavity boundary around the high-speed underwater vehicle. The cavitating flow around a blunt axisymmetric body very near the free surface is investigated in the present paper. The typical experiment is carried out in a launching system based on an SHPB device, and the numerical scheme is established on the basis of large eddy simulation (LES) and volume of fraction (VOF) methods. Unsteady behaviors such as air injection and shedding of the cloud cavity were obtained, and good agreement was achieved between the numerical and experimental results. The distinctions of evolution features between the cavities on the up and down sides are presented and analyzed. Firstly, strong injection of non-condensable air occurs and changes the media property inside the cavity, which makes the cavity much larger and more stable. Furthermore, because of the small distance between the vehicle and the free surface, the re-entry jet generated in the upper part is very thin and cannot cut off the main cavity clearly, which induces that the upper part of the cavity is approximately unchanged after the growth stage and no shedding phenomenon occurs inside it.

Keywords

Ventilated cavitation — Free surface — Large eddy simulation

[1]*Key Laboratory for Mechanics in Fluid Solid Coupling Systems, Institute of Mechanics, Chinese Academy of Sciences, Beijing, China*

***Corresponding author**: huangcg@imech.ac.cn

INTRODUCTION

The interaction between the cavitation region and the free surface is an important issue for the fast cruise of surface vehicles. Ventilated cavitation occurs as an extremely complicated problem if the free surface is close to the vehicle or the cavity boundary as Faltinsen mentioned [1]. The gas above the free surface can inject into the cavity, which may change the dynamic behaviors of the cavity significantly. The effect of wave elevation is also coupled with the distribution of cavitation region.

Relevant research works on the interactions between the free surface and the cavitating flow is very limited in literature. Most of these works were focused on the stable cavity, and the interfaces of the cavity and the free surface are separated between each other. Theoretical and numerical methods were established, and the influences of the free surface on the cavitating flow around hydrofoils and axisymmetric bodies are obtained [1–4]. On the other side, neglecting the influence of the free surface, the dynamic characteristics of the cloud cavitating flow are often linked with the motion of vortexes. Based on the experimental and numerical approaches, the evolution of cavities including growth, re-entry, shedding and collapse were gained [5–8].

The cavitating flow around a blunt axisymmetric body very near the free surface is investigated in the present paper. The typical experiment is carried out in a launching system based on an SHPB device, and the numerical scheme is established on the basis of large eddy simulation (LES) and volume of fraction (VOF) methods. The distinctions of evolution features between the cavities on the up and down sides are presented. The effects of the free surface and the gas injection on the cavity shape are analyzed.

1. EXPERIMENT SETUP

The experiment was performed by using a launching system (as shown in Figure 1) on the basis of the SHPB technology [8, 9], which can transiently accelerate the projectile with slight disturbance on the water. The projectile is driven by a strong stress wave. The acceleration process is very short which is about 200 s for 20m/s. Therefore the acceleration cannot be captured by using the high-speed camera. Moreover, because solid steel projectile is used which is rather heavy, the deceleration is also very small in the observation period. So the speed of projectile is considered approximately uniform for numerical simulation.The projectile used in this study is a blunt axisymmetric body. The total length is 150 mm, and the diameter is 37 mm. Photographs of typical cavitation can be obtained using a high-speed camera with 12000 fps. For the typical condition investigated in the present paper, the distance between the free surface and the up side of the projectile is 5mm, and the analysis of obtained images indicates that the speed is approximately uniform at 19.1 m/s. The cavitation number calculated as 0.537.

The cavity is nonaxisymmetrically affected by the free surface. Thus, the length on the upper and lower sides of the cavity is measured, as shown in Figure 2. The precision of the length and thickness is approximately a pixel of the image, which stands for about 0.65 mm.

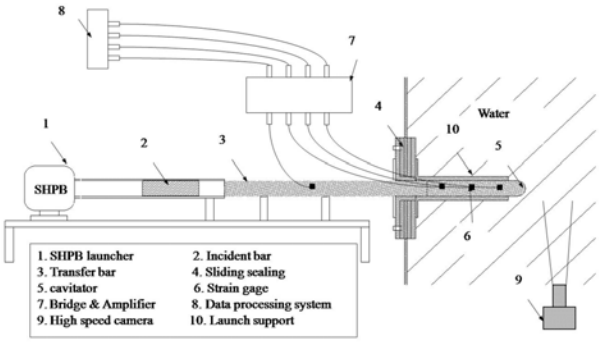

Figure 1. Underwater launch system

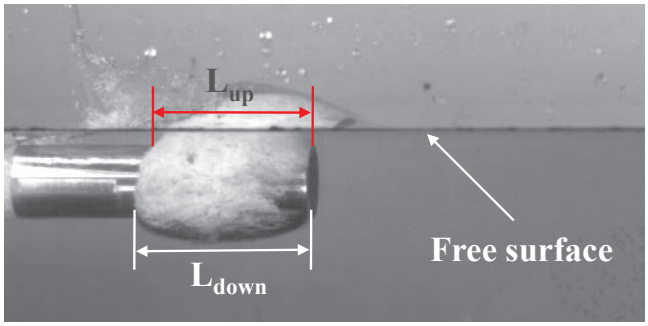

Figure 2. Typical cavitation photograph

2. NUMERICAL METHODS

2.1 Governing equations

To simulate the motions of liquid water and vapour and air, including the phase change, mixture/multiphase flow equations are adopted. Continuity and momentum equations for the mixture are established as follows.

$$\frac{\partial \rho}{\partial t} + \frac{\partial (\rho u_j)}{\partial x_j} = 0 \tag{1}$$

$$\frac{\partial (\rho u_i)}{\partial t} + \frac{\partial (\rho u_i u_j)}{\partial x_j} = -\frac{\partial p}{\partial x_j} + \frac{\partial}{\partial x_j}\left(\mu \frac{\partial u_i}{\partial x_j}\right) \tag{2}$$

where u_i is the velocity component in the i direction, and p is the pressure. Laminar viscosity μ is defined as a volume-weighted average of the three components as

$$\mu = (1-\alpha_v-\alpha_a)\mu_l + \alpha_v \mu_v + \alpha_a \mu_a \tag{3}$$

where α_v and α_a are the vapour and air volume fractions, respectively. Mixture density ρ is defined as

$$\rho = (1-\alpha_v-\alpha_a)\rho_l + \alpha_v \rho_v + \alpha_a \rho_a \tag{4}$$

The volume fractions of vapour and air are governed by the following mass transfer equations:

$$\frac{\partial (\rho_v \alpha_v)}{\partial t} + \frac{\partial (\rho_v \alpha_v u_j)}{\partial x_j} = \dot{m}^+ - \dot{m}^- \tag{5}$$

$$\frac{\partial (\rho_a \alpha_a)}{\partial t} + \frac{\partial (\rho_a \alpha_a u_j)}{\partial x_j} = 0 \tag{6}$$

where source terms $\dot{m}^+$ and $\dot{m}^-$ represent the mass transfer rate of evaporation and condensation, which are derived from the bubble dynamics equations of generalised RayleighPlesset equation by Zwart et al.[10] as follows.

$$\dot{m}^+ = F_{vap} \frac{3 a_{nuc}(1-\alpha_v)\rho_v}{R_B} \sqrt{\frac{2}{3}\frac{\max(p_v - p, 0)}{\rho_l}} \tag{7}$$

$$\dot{m}^- = F_{cond} \frac{3 \alpha_v \rho_v}{R_B} \sqrt{\frac{2}{3}\frac{\max(p - p_v, 0)}{\rho_l}} \tag{8}$$

where generalised bubble radius R_B is set at 10^{-6}m, nucleation site volume fraction a_{nuc} is set at 5×10^{-4}, the evaporation coefficient is set at 50 and the condensation coefficient is set at 0.01.

2.2 Simulation procedure

The governing equations are solved by a LES approach based on Smagorinsky-Lilly model. Unsteady numerical simulations are performed on the basis of finite volume method with coupled scheme by using the commercial CFD software ANSYS-FLUENT. The equations are discretised by a second-order implicit scheme in time and a bounded central differencing scheme in space. The pressure staggering option was selected for pressure interpolation with the modified high-resolution interface-capturing scheme used for the volume fraction. The unsteady cavitating flow simulations were started from a uniform flow field, and the time step was set at 10^{-5} s.

The computational domain is discretised with a block-structured grid, which is refined around the model and near the free surface, and only half of the model is considered (as shown in Figure 3). A semi-infinite projectile model was used, and the effect of the tail on the shoulder cavity is neglected. The cell number is approximately 4 million with good orthogonality. Independence analysis and validation of similar grid have been performed on a simulation of the typical evolution of cloud cavitating flow [8]. The model was fixed, with the free surface moving towards the model. The inlet velocity is set as 19.1 m/s, with no turbulent perturbations for the velocity inlet boundary condition.

3. RESULTS AND DISCUSSION

3.1 Overall cavities evolutions

From the experimental and numerical results, the quasi-periodic development of cavity shape is obtained. Photographs on typical moments of different stages are as shown in Fig.4, and the volume fraction of liquid water is 0.9 on the iso-surface. The contours of water volume fraction on the symmetric plane and wall surface are also given, in which the red

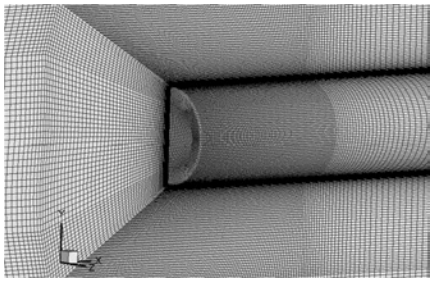

Figure 3. Mesh near the head of the projectile

color represents that the volume fraction is 1 while the blue color represents zero.

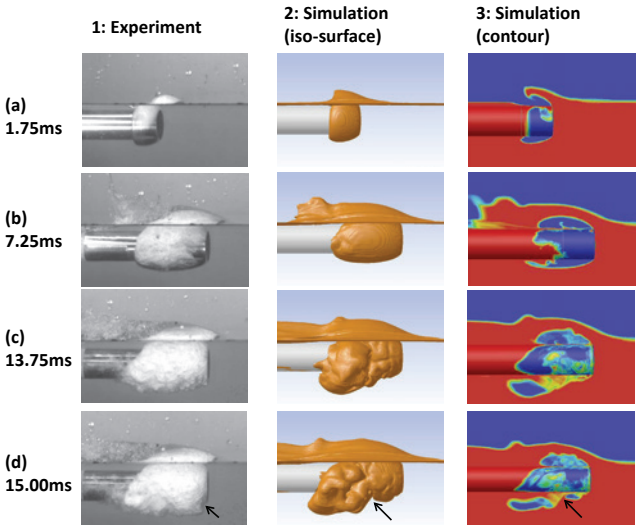

Figure 4. Time evolution of cavitation patterns (the breaking location is marked by the arrows in the bottom views)

The variations of cavity lengths on the up and down sides are as shown in Figure 5. The length development and variation of the obtained numerical results agree fairly with the experiments, including the breaking phenomenon of the lower side cavity and the relationship between cavities on upper and lower sides. These characteristics can affect the nature of the bubble within the media, the impact of the return jets and other characteristics of the unsteady factors.

Refer to the evolutions aforementioned, we can see the cavity on the upper side stays approximately stable, and its length varies in a very small range after the growth stage. The length variation on the lower side is similar with the case under the same cavitation number without the free surface but has much larger amplitude. These characteristics are relevant to the particularities of the current case, for example the free surface are close to the cavity boundary and the air above the free surface has injected into the cavity. These characteristics can affect the media property inside the cavity, and have impact on the re-entry jet and other instability factors, which will be analyzed and discussed in detail separately in the following contents.

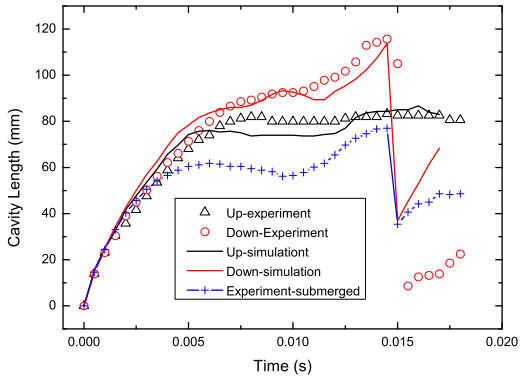

Figure 5. The comparison of the variation of cavity length between numerical and experimental results

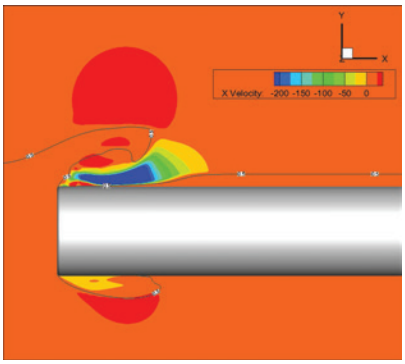

Figure 6. Flow field of the air entrainment at the beginning (the flow time is equal to 2ms, and the line represents the interfaces where the volume fraction of the liquid water is equal to 0.5, while the color represents the velocity in the X direction)

3.2 Air entrainment into the cavity

The thickness of the cavity increases gradually in the growth stage, and regions of free air space and the cavity will connect after the cavity boundary intersects with the free surface. Because the pressure above the free surface is about 1atm, which is much higher than the pressure inside the cavity, high-speed air entrainment forms in the connecting channel. At the beginning of the air entrainment, high-speed air flow impacts on the leading edge of the cavity, which raises the upper cavity boundary and thickens the cavity (as shown in Figure 6). At the same time, air also flows to the low pressure region inside the cavity on the lower side and fills it (as shown in Figure 7). The region influenced by the air entrainment is foam-like in the experiment photograph (as shown in Figure 4-1a), the shape of which is similar with the region with large negative Y velocity in numerical results (as shown in Figure 7).

Thereafter, the water layer between the cavity and the outside space is affected by gravity, and moves downward to

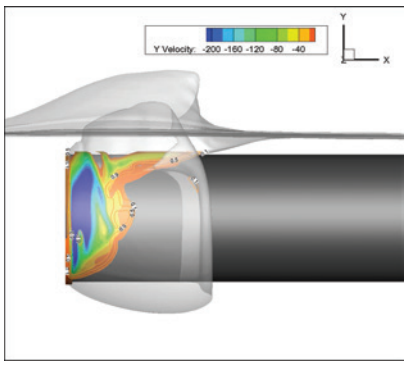

Figure 7. Distribution of the air entrainment at the beginning (the flow time is equal to 2ms, translucent surfaces represent the cavity boundary and the free surface, line represents the volume fraction of air, and the color represents the velocity in the Y direction)

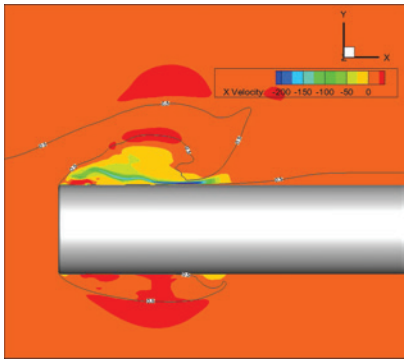

Figure 8. Flow field of the air entrainment at the end (the flow time is equal to 4ms, and the line represents the interfaces where the volume fraction of the liquid water is equal to 0.5, while the color represents the velocity in the X direction)

the wall. The reattachment occurs at the time of about 4ms, which ends the air entrainment finally. As shown in Figure 8, the water layer was curled under the joint effects of gravity and air entrainment, and the air entrainment is compressed just inside a very thin gap. The circular velocity inside the cavity also decreases remarkably at this moment (as shown in Figure 9). The whole air entrainment process lasts about 2ms in the cavity growth stage, carrying large amounts of air to fill the cavity. On the one hand, it increases the inner pressure significantly, so the inner pressure is actually remarkably higher than the saturation pressure in the natural cavitation bubbles, which can be considered as that the cavitation number is decreased. On the other hand, the ventilated air cannot condense, which will weaken the condensation and collapse processes on the cavity trailing edge remarkably, and will also increase the cavity length and stability.

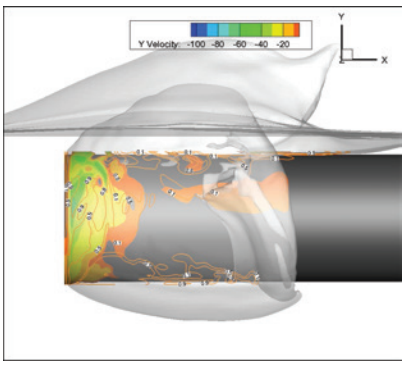

Figure 9. Distribution of the air entrainment at the end (the flow time is equal to 4ms, translucent surfaces represent the cavity boundary and the free surface, line represents the volume fraction of air, and the color represents the velocity in the Y direction)

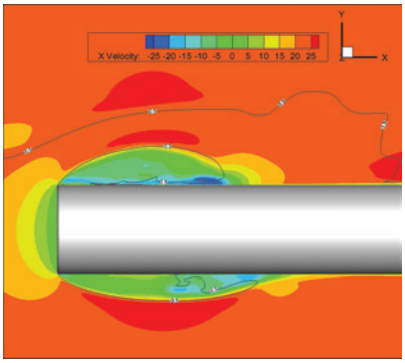

Figure 10. The velocity of the re-entry jet on the symmetric plane (the flow time is equal to 7ms, and the line represents the interfaces where the volume fraction of the liquid water is equal to 0.5, while the color represents the velocity in the X direction)

3.3 Influence on re-entry jets and cavity shedding

Strong adverse pressure gradient forms in the cavity growth stage in the area between the high pressure region at the cavity closure and the low pressure region inside the cavity. Flow detachment will occur, and re-entry jets is generated as a water layer flowing upstream near the wall inside the cavity. The cavity profile and the re-entry jet velocity on the symmetric plane are as shown in Figure 10. It demonstrates that velocity of the re-entry jet on the upper side is high but the water layer is very thin. In contrast, re-entry jet velocity on the lower sides is slower, but the water layer is much thicker (as shown in Figure 10). And the middle and lower parts of the cavity are significantly disturbed by the re-entry jet (as shown in Figure 11).

With the further development of the re-entry jet, the cavity on the upper side is cut off at first. However, because re-entry jet is very thin, there is only a small gap between

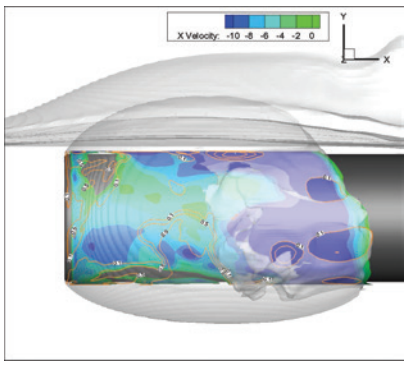

Figure 11. Shape of the re-entry jet (the flow time is equal to 7ms, translucent surfaces represent the cavity boundary and the free surface, line represents the volume fraction of air, and the color represents the velocity in the X direction

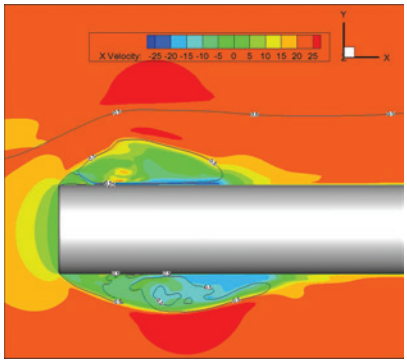

Figure 12. The velocity of the re-entry jet and cavity breaking on the upper side on the symmetric plane (the flow time is equal to 11ms, and the line represents the interfaces where the volume fraction of the liquid water is equal to 0.5, while the color represents the velocity in the X direction)

the newly incepted and the remaining cavities (as shown in Figure 12). The gap will be filled soon by the growth of the new cavity. In contrast, the re-entry jet in the lower part of the cavity is thick and cut off the cavity by intersecting with the outside cavity boundary. It is also seen in the experiment photograph (as shown in Figure 4-1b) that the upper part of the cavity is smooth while the middle and lower parts have many small holes on the surface.

When the re-entry jet reaches the leading edge of cavity on the lower side, the remaining bubbles only retain a small space of the origin cavity. A region with high content of liquid water can separate the new cavity form the remaining part, inducing obvious shedding phenomenon. However, only small fluctuation occurs on the cavity boundary on the upper side, and the cavity approximately remains in a constant area.

Aforementioned results indicate that, if the vehicle moves closely to the free surface, the water layer flowing around the

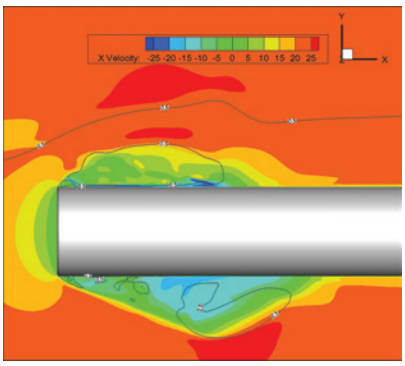

Figure 13. Cavity breaking on both sides on the symmetric plane (the flow time is equal to 13ms, and the line represents the interfaces where the volume fraction of the liquid water is equal to 0.5, while the color represents the velocity in the X direction)

upper side is thin and the restriction of water layer to the flow is weak. Thus, the re-entry jet generated does not also have enough strength and thickness to cut off the main cavity clearly, so notable fluctuation of cavity shape cannot be induced on the upper side. However, the influence of the free surface on the cavity on the lower side is relatively small, so powerful re-entry jet can be generated, and unsteady evolutions including breaking and shedding are still exist.

4. CONCLUSIONS

An experiment on the ventilated cloud cavitating flow around the axisymmetric projectile near the free surface has been presented in this paper. A relevant numerical simulation was performed based on VOF and LES methods. Unsteady behaviors such as air entrainment and shedding of the cloud cavity were obtained, and good agreement was achieved between the numerical and experimental results.

Strong air entrainment occurs when the cavity grows and contacts the free surface. The ventilated non-condensable air makes the cavity much larger and more stable than the cloud cavity under similar cavitation number without the influence of the free surface.

The upper part of the cavity is approximately unchanged after the growth stage and no shedding phenomenon occurs inside it. This is because the restriction of water layer to the flow flowing around the upper side is weak, and the re-entry jet generated in the upper part is very thin and cannot cut off the main cavity clearly.

However, there are still some differences on the phenomena after cavity shedding, and the current numerical simulation method should be further validated by comparing with classic experimental results of ventilation cavitation and also be improved in the future. Through other experimental and numerical results with various submergence, it is found that this specific phenomenon discussed in the present paper just may occur in a very small submergence range. The ventila-

tion dose not happen if the submergence is large, while the stable ventilated supercavity appears if the submergence is smaller. The detailed results with other submergence may be provided in other subsequent papers.

Moreover this present work can be extended to other shape vehicles including the hydrofoils, and the cavity may be controlled to remain stable by adjusting the distance between the vehicle and the free surface.

ACKNOWLEDGMENTS

This research was sponsored by National Natural Science Foundation of China (Grant numbers 11332011 & 11202215) and the Youth Innovation Promotion Association of CAS (Grant number 2015015).

REFERENCES

[1] O. M. Faltinsen and Y. A. Semenov. The effect of gravity and cavitation on a hydrofoil near the free surface. *Journal of Fluid Mechanics*, 597:371–394, 2008.

[2] S. Bal and S. A. Kinnas. A bem for the prediction of free surface effects on cavitating hydrofoils. *Computational Mechanics*, 28:260–274, 2002.

[3] S. Bal. High-speed submerged and surface piercing cavitating hydrofoils, including tandem case. *Ocean Engineering*, 34:1935–1946, 2007.

[4] E. Amromin. Analysis of body supercavitation in shallow water. *Ocean Engineering*, 34:1602–1606, 2007.

[5] B. Stutz and S. Legoupil. X-ray measurements within unsteady cavitation. *Experiments in Fluids*, 35:130–138, 2003.

[6] B. Ji, X. W. Luo, and Arndt R. E. A. Large eddy simulation and theoretical investigations of the transient cavitating vortical flow structure around a naca66 hydrofoil. *International Journal of Multiphase Flow*, 35:130–138, 2003.

[7] B. Roohi, A. P. Zahiri, and Passandideh-Fard M. Numerical simulation of cavitation around a two-dimensional hydrofoil using vof method and les turbulence model. *Applied Mathematical Modelling*, 37:6469–6488, 2013.

[8] X. Yu, C. Huang, T. Du, L. Liao, X. Wu, Z. Zheng, and Y. Wang. Study of characteristics of cloud cavity around axisymmetric projectile by large eddy simulation. *Journal of Fluids Engineering*, 136:051303, 2014.

[9] Y. Wei, Y. Wang, X. Fang, C. Huang, and Z. Duan. A scaled underwater launch system accomplished by stress wave propagation technique. *Chinese Physics Letters*, 28:024601, 2011.

[10] P. J. Zwart, A. G. Gerber, and T. Belarmri. A two-phase flow model for predicting cavitation dynamics. In *Fifth International Conference on Multiphase Flow*, Yokohama, Japan, 2004.